Evidence for a Solar System Origin of 3I/ATLAS and Related Small Bodies within World–Universe Cosmology

Vladimir S. Netchitailo
netchitailo.vs@gmail.com

Abstract

The object formally designated **C/2025 N1** (ATLAS) has been widely discussed as a candidate third interstellar object ("3I/ATLAS") due to its strongly hyperbolic trajectory. In standard celestial mechanics, an interstellar origin is inferred when the original barycentric eccentricity significantly exceeds unity prior to planetary perturbations. This interpretation, however, implicitly assumes that cometary dynamics are governed solely by gravitational forces and conventional outgassing.

In this work, we propose an alternative hypothesis: **C/2025 N1** (ATLAS) is not interstellar but a Solar System small body originating from the Oort Cloud, consistent with the framework of World–Universe Cosmology (WUC). We argue that its large excess velocity can be explained by a non-gravitational internal acceleration mechanism involving partial conversion of rotational energy of the nucleus into translational kinetic energy.

Within WUC, the Universe is structured as a hierarchy of interaction regimes—Macro-world (gravity), Large-world (extremely-weak interaction), Small-world (super-weak interaction), and Micro-world (weak interaction). Previous studies associate Ball Lightning [1] with Solar System Small Body (SB1) and interpret the Tunguska superbolide [2] as an SB2 analogue. Extending this hierarchy, we identify **C/2025 N1** (ATLAS) as an SB3 object. This model naturally accounts for its extreme hyperbolic excess velocity without invoking an interstellar origin and leads to specific, testable predictions regarding kinematics, activity, and radiation signatures.

We compare these predictions with observations of 'Oumuamua, **C/2019 Q4** (Borisov), and a growing population of low-albedo asteroids and "dark comets" exhibiting dust-poor outgassing.

1. Introduction

The Interplanetary Medium (IPM) comprises the matter and energy filling the Solar System, extending outward to the Heliopause—the boundary where the solar wind is balanced by the surrounding Interstellar Medium (ISM). Measurements by the Voyager spacecraft place this boundary at approximately 120 AU, although its shape is asymmetric, compressed in the direction of solar motion and extended in the polar regions.

Beyond the Heliopause lies the ISM. However, the physical and dynamical extent of the Solar System is not necessarily limited to this boundary. The Oort Cloud, a hypothesized reservoir of icy bodies, likely extends from $\sim 10^3$ AU to $\sim 10^5$ AU and remains gravitationally bound to the Sun. It is commonly divided into an inner disk-like component and a distant, nearly spherical outer component. Although often described as lying in interstellar space, the Oort Cloud is generally understood to consist of material formed within the early Solar System and later scattered outward by interactions with the giant planets.

Comets are traditionally classified into short-period (ecliptic) comets with orbits within ~10 AU and long-period comets (LPCs) with highly elongated orbits extending to thousands of AU. LPCs appear nearly isotropic in their arrival directions and are widely attributed to the Oort Cloud.

The discovery of objects on strongly hyperbolic trajectories—such as ‘Oumuamua and **C/2019 Q4** (Borisov)—has led to the prevailing interpretation that such bodies originate in the ISM. The designation of **C/2025 N1** (ATLAS) as a potential third interstellar object (“3I/ATLAS”) follows this paradigm.

However, this interpretation rests on a key assumption: that hyperbolic motion necessarily implies an extrasolar origin. In this paper, we challenge this assumption within the framework of World–Universe Cosmology. In WUC, the effective radius of the Solar System is estimated to be ∼96,000 AU, comparable to the outer extent of the Oort Cloud. From this perspective, the Oort Cloud remains an intrinsic component of the Solar System rather than a transitional boundary to interstellar space.

We therefore explore an alternative hypothesis: **C/2025 N1** (ATLAS) is a Solar System Small Body whose hyperbolic excess velocity arises from an internal, non-gravitational energy conversion mechanism, removing the need to invoke an interstellar origin.

2. Long-Period Comets

Astronomical observations since the mid-19th century have revealed numerous weakly hyperbolic comets, many of which are interpreted as Oort Cloud objects subsequently perturbed onto escape trajectories. In several well-studied cases, comets initially bound to the Solar System transitioned to unbound orbits following close encounters with giant planets. Notable examples include **C/1980 E1** (Bowell) and **C/2024 L5** (ATLAS), both of which acquired hyperbolic trajectories through planetary scattering.

Long-period comets (LPCs) are conventionally defined as bodies with orbital periods exceeding 200 years. A subset—very long-period comets—have orbital periods of millions of years and are believed to originate in the outer Oort Cloud. For example, **C/1999 F1** (Catalina) has an orbital period of several million years.

LPCs exhibit several well-established properties:

- **Orbital periods:** hundreds of years to millions of years
- **Dynamical origin:** perturbations by passing stars, molecular clouds, and galactic tides
- **Isotropic distribution:** reflecting the spherical structure of the Oort Cloud
- **Primitive composition:** high volatile content, leading to strong activity near the Sun

Recent surveys have expanded the known population of Oort Cloud comets to several thousand objects, a number expected to grow substantially with the Legacy Survey of Space and Time (LSST). Among these, **C/2014 UN271** (Bernardinelli–Bernstein) is the largest known Oort Cloud comet and exhibits **activity at unusually large heliocentric distances** (see **Table 1**).

A key observational result is that hyperbolic trajectories are not uncommon among LPCs. In most cases, their weak hyperbolicity can be explained by:

- planetary perturbations (e.g., scattering by Jupiter or Saturn), or
- non-gravitational forces driven by asymmetric outgassing

However, these mechanisms typically produce **only weakly hyperbolic orbits**, with eccentricities slightly exceeding unity ($e \gtrsim 1$). Even in extreme cases such as **C/1980 E1** (Bowell), the observed excess velocity remains modest and can be quantitatively explained within standard dynamical frameworks.

In contrast, **C/2025 N1** (ATLAS) exhibits an **extraordinarily large eccentricity** ($e \approx 6.14$), far beyond the range achievable through known gravitational or outgassing processes. This places it in a fundamentally different dynamical regime.

Table 1. Long-Period Comets with Extreme Aphelia

Comet	Inbound Aphelion (AU) Orbital period (Myr)	Outbound Aphelion (AU) Orbital period
C/1973 E1 (Kohoutek)	98,000 (~11 Myr)	3,700 (80,000 yr)
C/1999 F1 (Catalina)	54,000 (~4 Myr)	66,000 (~6 Myr)
C/2000 W1 (Utsunomiya–Jones)	70,000 (Myrs) e=0.9999996	1,670 (~24,000 yr)
C/2006 P1 (McNaught)	67,000 (~6 Myr)	4,100 (~92,600 yr)
C/2010 X1 (Elenin)	97,000 (Myrs)	
C/2010 U3 (Boattini)	34,000 (~2.2 Myr)	9,900 (~350,000 yr)
C/2011 L4 (PanSTARRS)	68,000 (Myrs)	4,500 (~107,000 yr)
C/2013 A1 (Siding Spring)	52,000 (Several Myr)	13,000 (~500,000 yr)
C/2014 UN_{271} (Bernardinelli–Bernstein)	42,000 (~3 Myr) e=0.99947	59,000 (~5.1 Myr) e=0.99967
C/2017 K2 (PanSTARRS)	51,200 (~4.1 Myr)	1,750 (~25,800 yr)
C/2017 T2 (PanSTARRS)	74,000 (~7 Myr)	3,000 (~55,000 yr)
C/2019 E3 (ATLAS)	65,200 (~5.9 Myr)	34,000
C/1980 E1 (Bowell)	75,000 (~7.1 Myr) e=1.066	Oort-cloud comet ejected by Jupiter, Hyperbolic, e>1.057
C/2013 US_{10} (Catalina)	38,000 (Several Myr)	Hyperbolic trajectory
C/2024 L5 (ATLAS)	Original barycentric $e \approx 0.999$	Oort-cloud comet ejected by Saturn, Hyperbolic, e>1.037
C/2023 A3 (Tsuchinshan–ATLAS)	≈380,000 (83 Myr) Original barycentric $e \approx 0.999$	Weakly hyperbolic, Future barycentric e≈ 1.001–1.003
C/2025 N1 (ATLAS)	Original barycentric $e > 1.01$	Ejected by the Sun, strongly hyperbolic trajectory, $e = 6.14$

We therefore argue that the distinction between typical hyperbolic comets and **C/2025 N1** (ATLAS) is qualitative rather than merely quantitative. Its extreme trajectory strongly suggests the presence of a powerful non-gravitational acceleration mechanism. Within WUC, this behavior is naturally interpreted as the result of internal energy conversion.

3. Hyperbolic Asteroids

Asteroids are conventionally defined as minor planets—solid bodies larger than meteoroids ($\gtrsim$1 m) that do not exhibit cometary activity. Most reside in the main asteroid belt between Mars and Jupiter and are composed primarily of rock and metal. However, modern observations increasingly reveal a continuum between asteroids and comets rather than a strict dichotomy.

A hyperbolic asteroid is a small body observed on an orbit with eccentricity $e > 1$, implying that it is not gravitationally bound to the Sun. Unlike comets, such objects initially show no detectable coma or outgassing, and their motion appears consistent with purely gravitational dynamics.

In practice, many objects initially classified as hyperbolic asteroids are later reclassified as comets once faint activity is detected. Examples include **C/2018 C2** (Lemmon) and **C/2018 F4** (PAN-STARRS), both of which exhibited delayed or weak cometary signatures. This highlights the observational challenge of distinguishing inactive comets from asteroids based on early data.

The most notable confirmed hyperbolic asteroid is ‘Oumuamua, which displayed no classical coma yet exhibited significant non-gravitational acceleration, likely driven by non-standard outgassing (e.g., H_2 or other low-visibility volatiles).

A key observational trend is that most hyperbolic small bodies are only **weakly unbound**, with eccentricities slightly above unity. Their trajectories can generally be explained by:

- gravitational perturbations,
- radiation pressure, or
- weak, often undetected outgassing

Thus, even among objects classified as asteroidal, strongly hyperbolic trajectories are rare and typically require additional physical explanation.

4. Small Solar System Bodies

Small Solar System Body (SSSB) is an object in the Solar System (SS) that is neither a planet nor a dwarf planet, nor a natural satellite. The term was first defined in 2006 by the International Astronomical Union (IAU) as follows: "*All other objects, except satellites, orbiting the Sun shall be referred to collectively as 'Small Solar System Bodies'*".

4.1. Dark Comets

The discovery of ‘Oumuamua revealed a new dynamical class of small bodies: objects that exhibit **non-gravitational acceleration without visible cometary activity**. Unlike classical comets, ‘Oumuamua showed **no detectable coma or dust tail**, yet its trajectory deviated measurably from a purely gravitational orbit.

In cometary physics, **dust particles** are micron- to sub-millimeter-sized solid grains released from the nucleus during volatile sublimation. These grains scatter sunlight and are responsible for the visible coma and dust tail observed in active comets. In contrast, gas species (e.g., H_2O, CO, H_2) are dynamically dominant and can produce non-gravitational acceleration through anisotropic outgassing. The absence of a detectable dust component, as observed in ‘Oumuamua, therefore implies either extremely low dust production or preferential release of gas without entrained solids, consistent with the emerging class of “**Dark Comets**.”

Non-Gravitational Acceleration without a Tail

The motion of ‘Oumuamua was tracked with high precision using facilities including the Hubble Space Telescope. These observations established that:

- **Direction:** The excess acceleration was consistently **radially outward from the Sun**.
- **Magnitude:** By early 2018, the object was displaced by ~40,000 km from its predicted gravitational trajectory.

This behavior implies the presence of a **continuous, low-level thrust**, analogous to cometary outgassing, but **without visible ejecta**.

Physical Interpretations

Several mechanisms have been proposed to explain this “invisible” acceleration:

Mechanism	Physical Basis
• Hydrogen outgassing	Release of trapped H_2 from irradiated ice
• Nitrogen ice sublimation	Evaporation of N_2 from Pluto-like fragments
• Radiation pressure	Momentum transfer from sunlight
• “Dark comet” activity	Dust-poor water vapor outgassing

The emerging consensus favors **hydrogen outgassing**, consistent with an **icy body whose surface layers were chemically altered by long-term cosmic-ray exposure in interstellar space**.

Dark Comets in the Solar System

Since the discovery of ‘Oumuamua, astronomers have identified a population of **“dark comets”**—Small Bodies that exhibit measurable non-gravitational accelerations but **lack visible comae or dust tails**. A notable example is **1998 KY_{26}** . It is a nearly spherical asteroid, approximately 11 meters in diameter and is a **fast rotator**, having a rotational period of only 5.35 minutes. It was first observed on 2 June 1998. In 2023, **1998 KY_{26}** was identified as a possible **dark comet**.. Dark comets are asteroids that exhibit comet-like acceleration, but visually appear as asteroids, with no coma or tail. Astronomers who study them believe the acceleration is caused by outgassing on the sunlit side. These Small Bodies suggest that:

- Low-level volatile release can occur without dust entrainment
- Outgassing may be spectrally or photometrically undetectable
- **Non-gravitational forces may be more common than previously recognized**

Thus, ‘Oumuamua may represent an **extreme case within a broader, previously unrecognized population**.

Contrast with Classical Cometary Behavior

The comet **C/2019 Q4** (Borisov) provides a key comparison. Unlike ‘Oumuamua, Borisov displayed **classical cometary activity**, including a prominent coma and dust tail driven by sublimation of volatiles such as H_2O and CO. Its non-gravitational acceleration is well explained by the **rocket effect**, in which anisotropic outgassing produces a recoil force on the nucleus. Observations further indicate a high abundance of carbon monoxide, allowing **activity to persist at large heliocentric distances**.

4.2. Low-Albedo Asteroids

The albedo in visible light ranges from about 0.9 to 0.95 for fresh snow to about **0.04 for charcoal**, **one of the darkest substances**. A key physical property linking these Small Bodies is their **extremely low albedo**. Typical values for dark bodies are 0.02 – 0.08 , significantly lower than that of the Moon (~0.12) or Earth (~0.30). So, **these asteroids are darker than charcoal**!

Main types of dark asteroids:

- **C-type (carbonaceous):** Most common (~75% of known asteroids). Rich in carbon, hydrated minerals Very primitive (early SS material). Examples: **253 Mathilde**, albedo ~0.044.
- **D-type:** Even darker and more **organic-rich**. Found in outer SS regions. Examples: **624 Hektor**, albedo 0.025; **911 Agamemnon**, albedo 0.037.
- **P-type:** low-reflectivity mixtures of carbon, silicates, and organics.

Their darkness is attributed to carbon-rich composition, complex organic residues, and long-term radiation processing.

Connection to interstellar objects:

- 1I/'Oumuamua (albedo 0.04 – 0.08).
- 2I/Borisov (albedo 0.03 – 0.04).
- 3I/ATLAS (albedo 0.02 – 0.06).

These objects are almost certainly **very dark**, but their exact albedo remains unconstrained. Such a low albedo implies either primitive composition (a carbon-rich, organic-coated surface) or surface processing (cosmic rays, UV, gamma radiation) over long timescales.

Observational Bias

Low-albedo bodies are difficult to detect due to their weak reflectivity and are often identified through infrared observations or deep sky surveys such as PanSTARRS. This introduces a strong observational bias, implying that many such Small Bodies likely remain undetected.

Synthesis

The combined evidence supports a unified interpretation in which:

- **Dark comets** represent a transitional population between asteroids and comets
- **Low albedo** reflects primitive composition and/or radiation processing
- **Non-gravitational acceleration** arises from dust-poor or dust-free outgassing

Within this framework, Small Bodies such as 'Oumuamua, **C/2019 Q4** (Borisov), and **C/2025 N1** (ATLAS) can be understood as members of a continuous population shaped by common physical processes.

4.3. 'Oumuamua

There is no detailed, high-resolution photograph of 'Oumuamua. Because the 'Oumuamua was so small and moving so fast, it appeared only as a single, faint point of light, even to our most powerful telescopes. The iconic "cigar-shaped" or "pancake-shaped" images seen in the media are artist's impressions based on mathematical models of how the object's brightness changed as it tumbled.

'Oumuamua was discovered about 40 days after it passed closest to the Sun. Major telescopes like Hubble could not be pointed at it until 'Oumuamua was already hundreds of millions of kilometers away and fading.

Because 'Oumuamua moved faster than gravity alone could explain, scientists have proposed several theories for this "non-gravitational acceleration." Since no visible comet tail was detected, the cause remains a subject of intense debate. There were proposed different mechanisms for non-gravitational acceleration:

1. Hydrogen Outgassing (Leading Natural Theory)

2. Nitrogen Iceberg

3. Solar Radiation Pressure. This theory suggests the acceleration was caused simply by the physical "push" of sunlight (photons) hitting the object's surface. **The Requirement**: For light alone to push 'Oumuamua this much, the object would have to be extremely thin—less than a millimeter thick—acting like a massive sail.

Implication: This led to the controversial suggestion that 'Oumuamua could be of artificial origin, such as a piece of advanced space debris or a probe. This suggestion was proposed based on eccentricity e=1.2 of its **outbound trajectory** after full Non-Gravitational Acceleration (NGA) during inbound trajectory. The first quantified value of 'Oumuamua NGA was obtained by M. Micheli, *et al.* [3]:

$$a_{\mathrm{NG}} \approx (4.9 \pm 0.2) \times 10^{-6}\ \mathrm{m}\ s^{-2}$$

that exceeds the NGA values for the classical comets by more than fifty times (see Section 4.6.), despite the absence of a detectable dust coma, demonstrating that significant recoil forces can arise from dust-poor or dust-free outgassing.

4.4. C/2019 Q4 (Borisov)

Unlike 'Oumuamua, where the acceleration was a mystery due to a lack of visible activity, **C/2019 Q4** (Borisov) behaved like a "textbook" comet. Its non-gravitational acceleration was clearly linked to the visible outgassing of gas and dust as it approached the Sun.

As Borisov got closer to the Sun, its ices (specifically water and carbon monoxide) sublimated directly into gas. This gas, along with dust particles, was ejected from the nucleus in "jets". These jets created a recoil force that pushed the comet slightly off its purely gravitational path.

Observations showed that Borisov was exceptionally rich in carbon monoxide (CO), which sublimates at much lower temperatures than water ice. This allowed it to remain active and continue accelerating even at great distances from the Sun.

Borisov was so "normal" that it helped astronomers understand what a typical interstellar comet looks like. Its acceleration allowed researchers to estimate its mass and density more accurately than they could for 'Oumuamua. The mechanism of its Non-Gravitational Acceleration $a_{NG} \sim 10^{-6}\ m\ s^{-2}$ (this value is much larger than the values for outgassing mechanism, see Section 4.6.) remains open.

4.5. C/2025 N1 (ATLAS)

Recent high-precision orbit determinations of **C/2025 N1** (ATLAS) provide strong evidence for **significant non-gravitational acceleration** (NGA) well above the levels typically observed in long-period comets. T. M. Eubanks *et al.* incorporated six additional observations obtained from two interplanetary spacecraft into the orbital solution. These measurements, acquired from vantage points and epochs inaccessible to ground-based observatories, reduced the formal uncertainties in the derived NGA parameters by approximately 20–40% compared to solutions based solely on terrestrial data collected between May and December 2025 [4].

Using this expanded dataset, they determined a **non-gravitational acceleration vector** (scaled to 1 AU) of:

$$(89.3 \pm 4.6) \times 10^{-9} \text{ au } day^{-2}$$

which corresponds to:

$$(1.79 \pm 0.09) \times 10^{-6} \text{ m } s^{-2}$$

Independent analyses by several authors yield comparable or even larger values, as summarized in **Table 2**.

Table 2. Reported Non-Gravitational Accelerations of **C/2025 N1** (ATLAS).

##	Authors	NGA ($m\ s^{-2}$)	Reference
1	Eubanks, T. M., *et al.*	$(1.79 \pm 0.09) \times 10^{-6}$	[4]
2	Neukart, F.	$(3.0 \pm 0.8) \times 10^{-5}$	[5]
3	Scarmato, T.	$\sim 0.5 \times 10^{-6}$	[6]
4	Ahuja, G., and Ganesh S.	$\sim 10^{-6}$	[7]
5	Spada, F., Królikowska, M. and Dones, L.	$(1.13 \pm 0.036) \times 10^{-6}$	[8]

According to *Jet Propulsion Laboratory: Small-Body Database Lookup*, the latest values of NGA for so named "interstellar comets" (Small Objects) are presented in **Table 3**:

Table 3. Latest Non-Gravitational Accelerations of "Interstellar Objects."

##	Small Objects	NGA ($m\ s^{-2}$)	Reference
1	1I/'Oumuamua	$(5.6 \pm 0.72) \times 10^{-6}$	[9]
2	2I/Borisov	$(0.98 \pm 0.08) \times 10^{-6}$	[10]
3	3I/ATLAS	$(1.06 \pm 0.024) \times 10^{-6}$	[11]

A central result emerging from these studies is that the characteristic magnitude of the non-gravitational acceleration satisfies:

$$a_{\text{NG}} \gtrsim 10^{-6} \text{ m } s^{-2}$$

This value is **one to four orders of magnitude larger** than the typical range observed in comets (Section 4.6.).

Implications

Such an unusually large acceleration cannot be readily explained by standard mechanisms:

- **Outgassing:** would require unrealistically high mass-loss rates or extreme anisotropy
- **Radiation pressure:** insufficient for an object of typical cometary size and mass
- **Thermal effects (Yarkovsky/YORP):** too weak by several orders of magnitude

Therefore, **C/2025 N1** (ATLAS) occupies **distinct dynamical regime**, in which the conventional framework of cometary physics appears insufficient.

This discrepancy strongly suggests the presence of an **additional or alternative acceleration mechanism**. Within the framework of WUC, such behavior is naturally interpreted as the result of an **internal energy conversion**, in which the rotational energy of the Nucleus is partially transformed into translational kinetic energy of the Small Body.

4.6. Sources of Non-Gravitational Accelerations

Non-gravitational accelerations (NGAs) are measurable deviations from purely gravitational motion, arising from internal or surface processes, as well as interactions with radiation and plasma. Although typically small in magnitude, NGAs play a crucial role in the orbital evolution of small bodies, particularly those on near-parabolic trajectories.

Principal sources of non-gravitational acceleration

(a) Outgassing (dominant for comets). Asymmetric sublimation of volatile ices produces reactive forces that alter the trajectory.

- Typical magnitude near 1 AU:

$$a_{\mathrm{NG}} \sim 10^{-10} \text{ to } 10^{-7} \text{ m } s^{-2}$$

- Effects:
  - shifts in perihelion timing (hours to days)
  - changes in eccentricity at the 10^{-7}– 10^{-6} level
  - modification of inferred original orbits

(b) Yarkovsky effect (thermal recoil). Anisotropic thermal emission from a rotating body produces a small thrust.

- Typical magnitude:

$$a_{\mathrm{Yark}} \sim 10^{-13} \text{ to } 10^{-10} \text{ m } s^{-2}$$

- Important for:
  - long-term orbital drift
  - near-Earth asteroid trajectory prediction

(c) YORP effect (rotational dynamics). Radiation and thermal emission exert torques that modify spin rate and axis orientation.

- Consequences:
  - spin-up or spin-down
  - changes in obliquity
  - possible structural disruption or fission
  - indirect influence on orbital evolution via altered outgassing geometry

(d) Radiation pressure. Momentum transfer from solar photons affects small or low-mass objects.

- Particularly relevant for:
  - very small bodies
  - low-density or high area-to-mass ratio objects

Summary

Non-gravitational accelerations in Solar System bodies arise primarily from **outgassing, radiation pressure, and thermal effects**. Their typical magnitudes (10^{-10}–10^{-7} m s^{-2}) are small but dynamically significant,

especially for long-period comets near the parabolic limit, where even minute perturbations can produce large changes in inferred orbital parameters.

However, these known mechanisms are **insufficient to explain strongly hyperbolic trajectories** such as that reported for **C/2025 N1** (ATLAS). This discrepancy motivates the exploration of alternative acceleration mechanisms, including those proposed within the framework of WUC.

4.7. Origin of Comets and Asteroids

Comets and asteroids are widely understood as remnants of the early Solar System (SS), formed approximately 4.6 billion years ago from the protoplanetary disk surrounding the young Sun. Their formation reflects the thermal gradient within this disk:

- Inner Solar System (high temperature): Formation of rocky and metallic bodies → asteroids.
- Outer Solar System (low temperature): Condensation of volatile ices mixed with dust → comets.

Asteroids primarily formed in the region now occupied by the asteroid belt, where gravitational perturbations from Jupiter inhibited accretion into a full-sized planet. Comets formed beyond the "snow line," where volatile compounds such as water, CO_2, methane, and ammonia could condense.

Subsequent gravitational interactions with the giant planets redistributed these bodies:

- **Kuiper Belt:** reservoir of short-period comets.
- **Oort Cloud:** source of long-period comets.

This standard model implies a **common origin in the protoplanetary disk**, with present-day differences arising from thermal history and dynamical evolution. At the same time, growing observational evidence supports a **continuum between asteroids and comets**, blurring traditional classification boundaries.

Key question. What is the ultimate origin of the material—dust, metals, ices, and complex molecules—that formed these primordial bodies? This question remains open and is central to alternative cosmological frameworks such as WUC.

5. Multiworld Framework [1]

The concept of multiple coexisting physical regimes has been previously hinted at in the literature. As noted by A. G. Oreshko, Pyotr Kapitsa suggested that *ball lightning may represent a "window" into another world* [12]. Motivated by this idea, we developed within WUC a hierarchical Multiworld framework consisting of **Macro-world, Large-world, Small-world, and Micro-world**.

In contrast to the standard cosmological paradigm invoking dark matter, WUC assumes that the World is composed of:

- **Ordinary Matter** (protons, electrons, photons, neutrinos), and
- **Universe-Created Matter (UCM)**, consisting of **Universe-Created Particles (UCPs)**.

These components interact through a hierarchy of interactions with different strengths and characteristic scales.

5.1. Macro-world (Gravitational Regime)

In WUC, gravity is described by a scale-dependent gravitational parameter:

$$G = G_0 \times Q^{-1}$$

where: $G_0 = \frac{a^2 c^4}{8\pi hc}$ is an extrapolated value of G at $Q = 1$, h is the Planck constant, c is a gravitodynamic constant, a is a basic length unit:

$$a = 1.7705641 \times 10^{-14}\, m$$

Q in the present Epoch equals $Q = 0.759972 \times 10^{40}$. The corresponding characteristic scale (radius of the World R) is:

$$R = a \times Q = 1.34558 \times 10^{26}\, m$$

The total mass and average critical density of the Macro-world are:

$$M_{\text{MW}} = 6\pi^2 m_0 \times Q^2 = 4.27 \times 10^{53}\ \text{kg}$$

$$\rho_{\text{MW}} = 3\rho_0 \times Q^{-1} = 8.88 \times 10^{-27}\, kg\, m^{-3}$$

where m_0 is a basic mass unit: $m_0 = h/ac$ and ρ_0 is a basic density unit: $\rho_0 = h/ca^4$.

5.2. Hierarchy of Interactions

WUC introduces three additional interactions beyond gravity: Weak, Super-Weak, and Extremely-Weak, characterized by the following parameters respectively:

$$G_W = G_O \times Q^{-1/4}$$

$$G_{SW} = G_O \times Q^{-1/2}$$

$$G_{EW} = G_O \times Q^{-3/4}$$

Each interaction defines the integrity and scale of a corresponding "world" (see **Table 4**).

5.3. Large-world (Extremely-Weak Interaction)

The Large-world is governed by the extremely-weak interaction, approximately **10 orders of magnitude stronger than gravity**. Its characteristic range is:

$$R_{EW} = a \times Q^{3/4} = 1.44 \times 10^{16}\ \text{m} \approx 1.52\ \text{ly} \approx 96{,}335\ \text{AU}.$$

Table 4. Parameters of the Multiworld.

Type of world	Type of Interaction	Rel. Interaction Parameter, G/G_0	Rel. Range of Interact, R_{max}/a	Rel. Mass, $M_{max}/4\pi m_0$	Rel. Density, $\rho/3\rho_0$
Macro-world	Gravity	Q^{-1}	Q	$1.5\pi \times Q^2$	Q^{-1}
Large-world	Extremely-weak	$Q^{-3/4}$	$Q^{3/4}$	$Q^{3/2}$	$Q^{-3/4}$
Small-world	Super-weak	$Q^{-1/2}$	$Q^{1/2}$	Q	$Q^{-1/2}$
Micro-world	Weak	$Q^{-1/4}$	$Q^{1/4}$	$Q^{1/2}$	$Q^{-1/4}$

Within WUC, this scale defines the boundary of **Extra-Solar Systems** (ESS), interpreted as spherical structures separating Solar-type systems from the Interstellar Medium.

The maximum total mass of such a system is:

$$M_{ESS} = 4\pi m_0 \times Q^{3/2} = 1.04 \times 10^{33}\ \text{kg} \approx 523\, M_\odot$$

with a corresponding maximum stellar mass:

$$M_{\text{Star}} = 1/3\, M_{ESS} \approx 174\, M_{\odot}$$

The average density:

$$\rho_{EW} = 3\rho_0 \times Q^{-3/4} = 8.29 \times 10^{-17}\ \text{kg}\, m^{-3}$$

exceeds the critical density by ten orders of magnitude.

5.4. Small-world (Super-Weak Interaction)

The Small-world is governed by the super-weak interaction, approximately **20 orders of magnitude stronger than gravity**. Its characteristic range is:

$$R_{SW} = a \times Q^{1/2} = 1.54 \times 10^{6}\ \text{m}$$

The maximum mass and density are:

$$M_{SW} = 4\pi m_0 Q = 1.19 \times 10^{13}\ \text{kg}$$

$$\rho_{SW} = 3\rho_0 Q^{-1/2} = 7.74 \times 10^{-7}\ \text{kg}\, m^{-3}$$

Within this framework:

- **Ball Lightning** → Small Body SB1[1]
- **Tunguska Superbolide** → Small Body SB2 [2]
- **C/2025 N1** (ATLAS) → **Small Body** SB3

Thus, **C/2025 N1** (ATLAS) is interpreted as a higher-order Solar System **Small Body**, whose anomalous dynamics arise from internal processes associated with UCM Nucleus..

Notably, the concept of **Super-weak interactions** was also explored by L. Wolfenstein [13], providing partial conceptual precedent.

5.5. Micro-world (Weak Interaction)

The Micro-world is governed by an interaction approximately **30 orders of magnitude stronger than gravity**, with range:

$$R_W = a \times Q^{1/4} = 1.65 \times 10^{-4}\ \text{m}.$$

This scale is many orders of magnitude larger than the conventional weak nuclear force range, implying a fundamentally different interaction regime within WUC.

The maximum mass is:

$$M_W = 4\pi m_0 \times Q^{1/2} = 1.37 \times 10^{-7}\ \text{kg} \approx 6.28\, M_{\text{Pl}},$$

and the density:

$$\rho_W = 3\rho_0 \times Q^{-1/4} = 7.23 \times 10^{3}\ \text{kg}\, m^{-3}$$

Micro-world objects, with masses about the Planck mass M_{Pl} (including dust particles in WUC), are proposed as the **fundamental building blocks of all macroscopic structures**.

5.6. Cosmic Bubbles

Within WUC, all four regimes—Macro, Large, Small, and Micro—are interpreted as **Cosmic Bubbles** (CBs) with well-defined boundaries characterized by a universal surface energy density:

$$\sigma_0 = \frac{hc}{a^3}$$

The total energy E_{CB} of a Cosmic Bubble of radius R_{CB} is [14]:

$$E_{CB} = 4\pi\sigma_0 R_{CB}^2$$

This relation provides a unifying description of structure formation across all scales, linking geometry, energy, and interaction strength.

6. Orbital Parameters of Solar System Bodies

In celestial mechanics, there is no sharply defined maximum cometary aphelion, as long-period orbits are highly sensitive to perturbations and observational uncertainties. Nevertheless, empirical evidence suggests a practical upper limit of order

$$R_{\max} \sim 10^5 \text{ AU} \approx 1.6 \text{ ly},$$

as illustrated by the comets listed in **Table 1.**

6.1. Solar System Hill Sphere (Galactic Context)

The Hill sphere defines the region within which the gravitational influence of a system dominates over external tidal forces. For SS embedded in the Milky Way, the Hill radius R_H can be approximated as

$$R_H = R_{\text{GC}} \left(\frac{M_{\text{SS}}}{3M_{\text{MW}}} \right)^{1/3}$$

where:

- $R_{\text{GC}} \approx 26.7$ kly is the Galactocentric distance of the Sun,
- $M_{\text{SS}} \approx 2 \times 10^{30}$ kg is the Solar System mass,
- $M_{\text{MW}} \approx 1.15 \times 10^{12} M_{\odot}$ is the enclosed Galactic mass.

This yields

$$R_H \approx 1.67 \times 10^{16} \text{ m} \approx 1.11 \times 10^5 \text{ AU} \approx 1.76 \text{ ly}.$$

Within the framework of WUC (Section 5), the characteristic Large-world scale is

$$R_{\text{EW}} = 1.44 \times 10^{16} \text{ m} \approx 0.963 \times 10^5 \text{ AU} \approx 1.52 \text{ ly}.$$

The close agreement between R_H and R_{EW} suggests that:

- the outer boundary of the Oort Cloud lies near $\sim 10^5$AU,
- stable cometary aphelia significantly beyond this scale are dynamically disfavored.

The corresponding maximum orbital period is

$$T = \sqrt{\frac{\pi^2 R_{\text{EW}}^3}{2GM_{\odot}}} \approx 15 \text{ Myr}$$

consistent with the longest reliably determined periods of long-period comets (**Table 1**).

The extremely large aphelion (~380,000 AU) and orbital period (~83 Myr) sometimes reported for **C/2023 A3** (Tsuchinshan–ATLAS) are likely influenced by:

- observational uncertainties, and
- non-gravitational perturbations.

For comparison, the distance to Proxima Centauri (~4.24 ly) highlights that such orbital solutions approach interstellar scales.

In standard astrophysics, the Solar System boundary is often associated with the Heliopause (~120 AU). In contrast, within WUC the effective boundary is set by the Large-world scale (~10^5 AU), consistent with the observed cutoff in comet aphelia.

No Solar System comet has a securely determined original barycentric aphelion exceeding ~10^5 AU; larger formal values arise naturally from uncertainties in near-parabolic orbit solutions.

6.2. Motion with Non-Gravitational Acceleration

To examine the dynamical impact of sustained non-gravitational acceleration (NGA), consider radial motion under solar gravity plus a constant outward acceleration a_{NG}:

$$\frac{d^2r}{dt^2} = -\frac{GM_\odot}{r^2} + a_{\mathrm{NG}},$$

with initial condition

$$\frac{dr}{dt}\,|_{r=r_0} = 0.$$

Integration yields

$$v^2 = 2\left[GM_\odot\left(\frac{1}{r} - \frac{1}{r_0}\right) + a_{\mathrm{NG}}(r_0 - r)\right].$$

For $r \ll r_0$, this simplifies to

$$v^2 \approx 2\left(\frac{GM_\odot}{r} + a_{\mathrm{NG}} r_0\right).$$

Application to C/2025 N1 (ATLAS)

Taking the perihelion distance

$$r_p = 1.35645\ \mathrm{AU} \approx 2.03 \times 10^{11}\ \mathrm{m},$$

the gravitational contribution alone yields

$$v_{\mathrm{grav}} \approx 3.62 \times 10^4\ \mathrm{m\ s^{-1}}$$

The observed maximum velocity is

$$v_{\mathrm{max}} \approx 6.83 \times 10^4\ \mathrm{m\ s^{-1}}$$

Thus, the excess component satisfies

$$v_{\mathrm{NG}}^2 = v_{max}^2 - v_{\mathrm{grav}}^2 \approx 3.36 \times 10^9\ m^2 s^{-2}$$

Assuming the NGA acts over a characteristic distance comparable to the Large-world scale,

$$r_0 \approx R_{\mathrm{EW}} = 1.44 \times 10^{16}\ \mathrm{m}$$

we obtain

$$a_{\mathrm{NG}} \approx \frac{v_{\mathrm{NG}}^2}{2r_0} \approx 1.17 \times 10^{-7}\ \mathrm{m\ s^{-2}}$$

This represents a **lower bound**, corresponding to acceleration acting over the maximum distance r_0. Even in this limiting case, the required acceleration lies at the upper end of—or exceeds—the typical range for cometary non-gravitational effects (10^{-10}–10^{-7} m s^{-2}).

However, directly inferred values for **C/2025 N1** (ATLAS) (Section 4.5) are of order

$$a_{\mathrm{NG}} \sim 10^{-6}\ m\ s^{-2}$$

clearly exceeding expectations from standard outgassing.

Conclusion

This analysis shows that:

- sustained non-gravitational acceleration can significantly modify cometary velocities,
- the magnitude required for **C/2025 N1** (ATLAS) exceeds that attainable by conventional mechanisms,
- a fundamentally different physical process must therefore be considered.

Within WUC, this is naturally interpreted as internal energy conversion, whereby rotational energy of the Nucleus is transformed into translational kinetic energy of the Small Body.

Moreover, weaker analogues of this process may contribute to the dynamics of other long-period comets, suggesting a broader role for non-gravitational acceleration than traditionally assumed.

6.3. Gravitationally Rounded Objects in the Solar System

Within WUC, all gravitationally rounded bodies—from planets to galaxy clusters—are proposed to contain cores composed of Universe-Created Matter (UCM). These cores consist of Universe-Created Particles (UCPs) undergoing continuous self-annihilation, forming **Self-Annihilating Reactors** (SARs) that function as persistent internal energy sources.

A representative lower bound for gravitational rounding in the Solar System is Saturn's moon Mimas, with:

- Mean radius: 198.2 ± 0.4 km
- Mass: 3.75×10^{19} kg
- Mean density: $\sim 1.15 \times 10^{3}$ kg m^{-3}
- Surface temperature: ~ 64 K

The observed temperature exceeds that expected from solar heating alone. Within WUC, this discrepancy is attributed to internal energy generation within the UCM core. Even at relatively low densities ($\sim 10^{3}$ kg m^{-3}), self-annihilation processes may remain effective.

Extending this concept, SARs are proposed to operate in all planetary bodies, including Earth, providing energy for:

- volcanism,
- seismic activity, and
- long-term geological evolution.

6.4. Tunguska Superbolide

The Tunguska event is commonly interpreted as the atmospheric disruption of a $\sim$ 50–60 m body, releasing $\sim$ 3–30 Mt TNT equivalent at an altitude of 5–10 km without forming an impact crater. Such events belong to the class of airbursts (fireballs or bolides), with the most energetic classified as superbolides.

Meteoroids enter Earth's atmosphere at velocities $\geq$11 km/s, compressing the air ahead of them and generating extreme temperatures through adiabatic heating (**ram pressure**). This process leads to ablation, fragmentation, or explosive disruption.

WUC Interpretation

Within WUC, the Tunguska object (SB2) is interpreted as follows:

- it possessed a low-density UCM core ($<10^3$ kg m^{-3}),
- under normal conditions, self-annihilation was inefficient, allowing stability in space,
- atmospheric entry increased core density via ram pressure,
- a critical threshold triggered rapid self-annihilation, producing explosive energy release.

The estimated maximum energy

$$E_{\mathrm{SB2}} \approx 1.26 \times 10^{17}\ \mathrm{J}$$

implies a core volume

$$V_{\mathrm{core}} \approx 0.4\ m^3$$

corresponding to a characteristic diameter

$$D_{\mathrm{core}} \sim 1\ \mathrm{m}.$$

Thus, SB2 bodies are interpreted as metastable UCM structures capable of rapid energy release under external perturbations.

7. Solar System Small Bodies in WUC

7.1. Origin of Solar System Small Bodies

In **WUC**, Ecliptic Small Bodies (SBs) were produced by the Sun as the result of Volcanic Rotational Fission (VRF) of the Sun's UCM Core 4.57 Byr ago [1].

Nearly isotropic SBs were produced by Giant Planets with different directions of their rotational axes (which are, in fact, "Failed stars") as the result of VRF of their UCM cores 4.57 Byr ago.

UCM cores of satellite objects can be any size from micrometers to thousands of km. Satellites are rocky or icy bodies as the result of the self-annihilation of UCPs inside of their cores with a density $\gtrsim 10^3\ kg\ m^{-3}$.

All chemical elements, compositions, and radiative outputs are generated in situ through UCPs self-annihilation within UCM cores of asteroids and comets. Formation of all objects in SS has a good explanation.

In case when the density of UCM cores of satellite is $< 10^3\ kg\ m^{-3}$ the self-annihilation process is not efficient. Then, there is a possibility of stable UCM Bolides (SB2), which are the analog of Ball Lightnings (SB1) with much larger internal energy.

7.2. Characteristics of Solar System Small Bodies

In WUC, **Small Bodies** (SBs) governed by the **super-weak interaction**. Its characteristic interaction range is:

$$R_{SW} = a \times Q^{1/2} \approx 1.54 \times 10^3\ \mathrm{km},$$

The theoretical maximum Small-world mass is:

$$M_{SW} = 1.19 \times 10^{13}\ \mathrm{kg}$$

Small Bodies consist of **Nucleuses** and **Inner Comae.** Nucleuses are Rotating Balls made of UCM with density in the range from 3.44 $kg\ m^{-3}$ up to $\sim 10^3\ kg\ m^{-3}$, at different rotation speeds up to the maximum speed at the Nucleus equator equals to the escape velocity.

The range of Weak interaction for particles UCF1 (1.3 TeV) is:

$$R_{UCF1}^{W} = 0.88 \times 10^{-8}\ m$$

and a calculated minimum particles concentration is:

$$n_{UCF1} = 1.47 \times 10^{24}\ m^{-3}\ .$$

Considering the rest energy of UCF1:

$$E_{UCF1} = 1.315\ TeV = 2.11 \times 10^{-7}\ J\ ,$$

we can calculate the minimum energy density of UCM core:

$$\rho_{UCF1} = 3.1 \times 10^{17}\ J/m^3$$

that is equivalent to the mass density of $\mathbf{3.44\ kg\ m^{-3}}$ that is not enough for the efficient self-annihilation.

Inner Comae have different diameters D_{IC} in the range of $\sim 10^3\ km$ up to the maximum diameter:

$$D_{IC} = 2R_{SW} \approx 3.1 \times 10^3\ km$$

Micro-world Connection: Dust and Coma Formation

The weak-interaction scale:

$$R_W \approx 1.65 \times 10^{-4}\ m \approx 165\ \mu m$$

matches the observed diameters of large dust grains D_{DG} in the inner comae [15] up to the maximum diameter D_{max} :

$$D_{max} = 2R_W \approx 330\ \mu m$$

This suggests that:

- **Micro-world objects (UCM fragments)** are continuously generated due to the Rotational Fission of Nuclei made of UCM,
- These fragments evolve into dust grains and volatiles via UCPs self-annihilation,
- The Inner comae are thus a direct manifestation of internal UCM processes.

Micro-Volcanism (MiV) Mechanism

Within WUC, the activity of SBs is driven by **recurrent MiVs** , governed by the following cycle:

1. **Energy Release Phase**
   - The UCM core ejects material,
   - A small fraction of mass is lost,
   - A significant fraction of rotational angular momentum is dissipated.
2. **Accumulation Phase**
   - The core absorbs UCPs from the environment,
   - Mass increases as $M \propto \tau$,
   - Angular momentum increases faster $L \propto \tau^{3/2}$.
3. **Instability Threshold**
   - When rotational velocity of core approaches the escape velocity a new MiV event is triggered.
4. **Continuous Outflow**
   - "Wind particles" analogous to solar wind form the inner coma,
   - Dust grains and volatiles are continuously replenished.

Energy Conversion Mechanism

A key feature of the model is the **conversion of rotational energy into translational kinetic energy**:

- MiVs generate internal torques,
- These torques reduce rotational energy of cores while increasing their translational kinetic energy,
- The process is analogous to a rotating body converting spin into linear motion under frictional interaction.

This mechanism naturally explains:

- the **large non-gravitational acceleration** (Section 4.5.),
- the **enhanced perihelion velocity** (Section 6.2.),
- the **stability of the acceleration over time**.

Importantly, the SB Nucleus is assumed to rotate at a **near-critical equatorial velocity**, approximately equal to its escape velocity, maintaining a quasi-steady energy conversion regime.

Synthesis

Within the WUC framework:

- **C/2025 N1** (ATLAS) is interpreted as a **Small-world Body** (SB3),
- Its coma, dust production, and dynamics arise from **internal UCM processes**,
- Its anomalous trajectory is explained by **continuous internal energy conversion**, rather than external forces alone.

This interpretation provides a **unified explanation** linking:

- cometary activity,
- non-gravitational acceleration, and
- hyperbolic motion.

7.3. Nucleus of Small Body

Estimates of the Nucleus properties of **C/2025 N1** (ATLAS) are **highly model-dependent**. Reported values include [16]:

- Density: $\rho \approx 200–600\ \mathrm{kg}\, m^{-3}$
- Mass: $M \approx 4.4 \times 10^{10}\ \mathrm{kg}$
- Diameter: $D \approx 0.520 – 0.748\ \mathrm{km}$

However, within the present framework, the **only directly measured parameters** are:

- Rotation period: $T = (16.16 \pm 0.01)\ \mathrm{h}$
- Diameter (Hubble): $D_H = 0.32 - 5.6\ km$

Rotation-Constrained Density $\boldsymbol{\rho}$

Assuming that the equatorial velocity equals the escape velocity $v = v_{esc}$

$$v^2 = \frac{2GM}{R} = \frac{8\pi G\rho}{3}R^2$$

we obtain:

$$\omega = \frac{v}{R} = \sqrt{\frac{8\pi G\rho}{3}} = \frac{2\pi}{T}$$

This yields a density depending **only on the rotation period**:

$$\rho = \frac{3\pi}{2GT^2}$$

For $T = 16.16$ h:

$$\rho \approx 20.9 \text{ kg } m^{-3}$$

Implications

- $\rho \gg 3.44 \text{ kg } m^{-3}$ (minimum UCM core density)
- $\rho \ll 10^3 \text{ kg } m^{-3}$ (efficient SAR threshold)

Thus, the Nucleus is **long-term stable**, with **low-rate self-annihilation**.

Size and Mass Constraints

Maximum possible radius (using Small-world mass limit $M_{SW} = 1.19 \times 10^{13}$ kg):

$$R_{\max} \approx 5.15 \text{ km} \quad D_{\max} \approx 10.3 \text{ km}$$

For the reported mass 4.4×10^{10} kg:

$$R \approx 0.80 \text{ km} \qquad D \approx 1.6 \text{ km}$$

Using the observational upper bound $R_H \leq 2.8$ km [37], the corresponding mass is:

$$M_H \lesssim 1.92 \times 10^{12} \text{ kg}$$

These values define a **physically consistent parameter space** for the Nucleus.

Rotational Energy

For $R_H = 2.8$ km:

$$v = \omega R_H \approx 0.30 \text{ m } s^{-1}$$
$$E_{\text{rot}} = \frac{1}{5}Mv^2 \approx 3.5 \times 10^{10} \text{ J}$$

Within WUC, this rotational energy of the Nucleus acts as a **reservoir for conversion into translational kinetic energy** of **C/2025 N1** (ATLAS) contributing to the observed non-gravitational acceleration.

8. WUC Explanation of C/2025 N1 (ATLAS) Observations

8.1. Key Observations of C/2025 N1 (ATLAS)

C/2025 N1 (ATLAS) appears distinctly diffuse in telescope images, indicating that its nucleus is surrounded by a coma—a cloud of gas and dust produced by outgassing. Coma maps of H_2O, CO_2, and CH_4 (**Figure 1**) reveal structured emission with a modest anti-sunward extension. Within the WUC framework, the inner coma has a characteristic scale of several thousand kilometers that is in good agreement with the observed data [17].

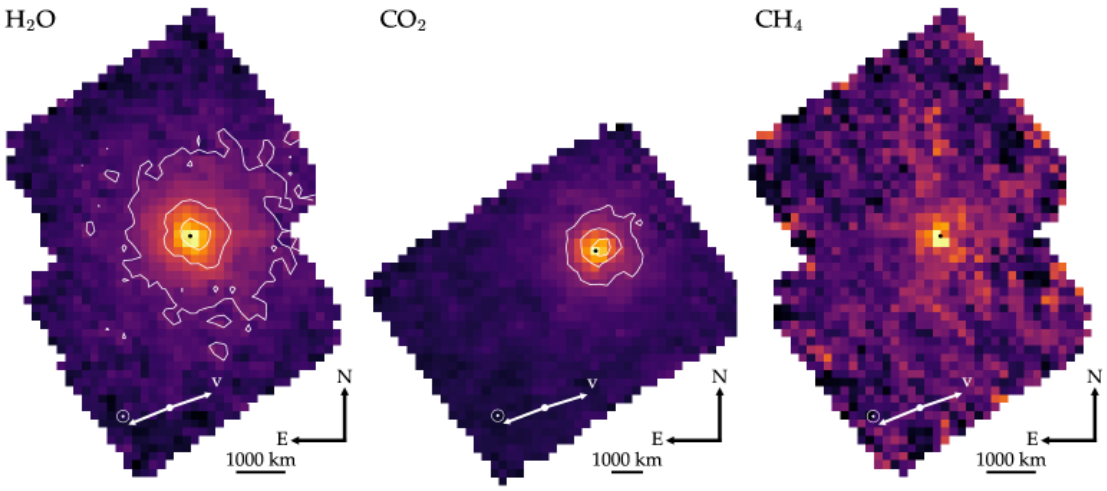

Figure 1. Coma maps of H_2O, CO_2, and CH_4, computed as the integrated emission flux across the corresponding fluorescence bands for Observations 6, 15, and 13, respectively. The sunward and target velocity directions are denoted by the white arrows. The target centroids, computed as the photocenter in the median-stacked images, are marked with the black points. For H_2O and CO_2, the white contours correspond to emission levels of 75%, 50%, and 25% relative to the maximum value and illustrate the slight anti-sunward extension of the respective comae. The precise spatial distribution of CH_4 in the near-nucleus region is poorly constrained due to the low signal-to-noise ratio of the data. Adapted from [17].

Space-based imaging further confirms typical cometary morphology. Observations from ESA's *JUICE* mission show a bright coma, extended tail, and fine structures including jets, filaments, and streams [18] (**Figure 2**). Although often described as an interstellar visitor, its observed behavior is consistent with that of an active comet.

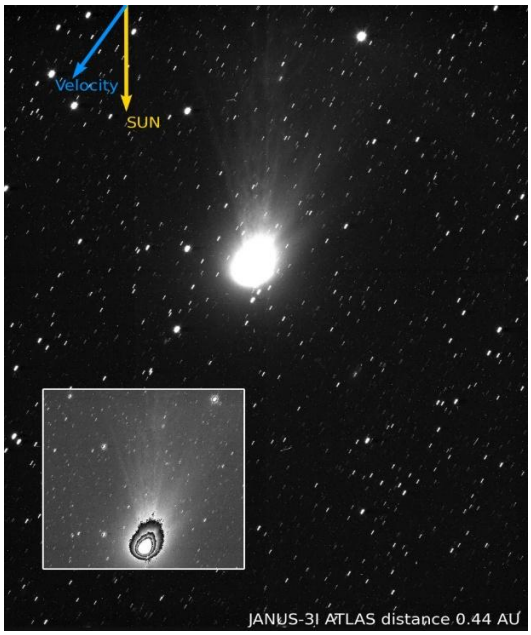

Figure 2. The arrows in the top left indicate the direction in which the comet was moving (blue) and the relative direction of the Sun (yellow). Adapted from [18].

Ultraviolet observations obtained by NASA's *Europa Clipper* spacecraft (**Figure 3**) reveal a compact UV-bright region near the nucleus, although its precise size remains unconstrained due to instrumental limitations [19].

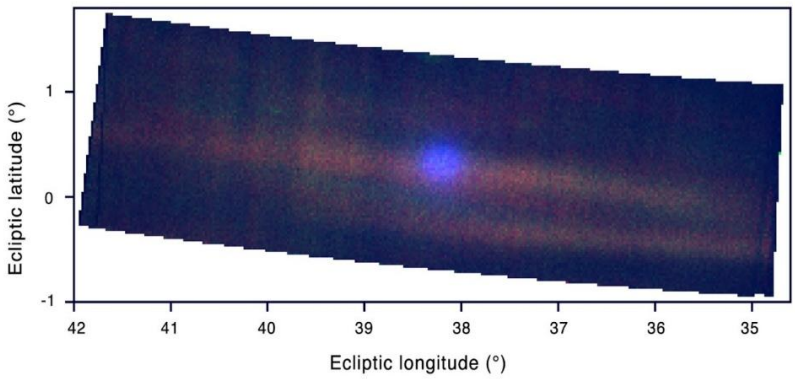

Figure 3. Interstellar comet 3I/ATLAS is seen in this composite image captured on Nov. 6, 2025, by the Europa Ultraviolet Spectrograph instrument on NASA's Europa Clipper spacecraft instrument, from a distance of around 103 million miles (164 million kilometers). Adapted from [19].

X-ray observations by *XMM-Newton* and *XRISM* [20], [21], [22] (**Figure 4**) detect:

- extended emission in the 0.3–1.0 keV range,
- spatial scales up to $\sim 4 \times 10^5$ km,
- spectral features associated with C, N, and O.

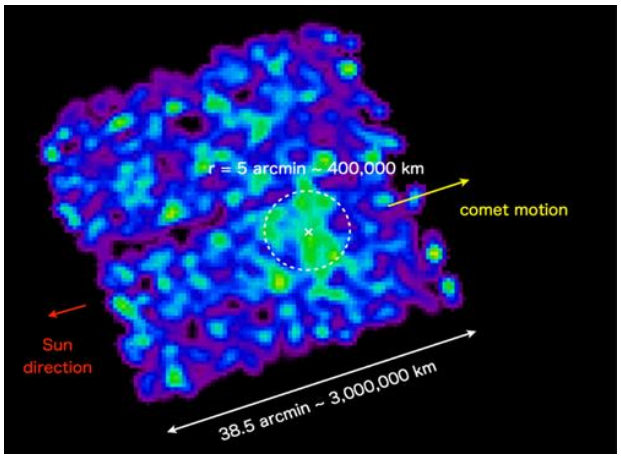

Figure 4. An image of comet 3I/ATLAS from the X-Ray Imaging and Spectroscopy Mission (XRISM). Image credit: JAXA.

These emissions are conventionally interpreted as solar wind charge exchange with neutral coma gas. Notably, X-ray diagnostics are particularly sensitive to hydrogen and nitrogen species that are difficult to detect at optical and infrared wavelengths.

8.2. Cosmic-Ray Processing Signatures

Spectroscopic observations using *JWST/NIRSpec* and *SPHEREx* reveal an unusually high CO_2 enrichment:

$$CO_2/H_2O = 7.6 \pm 0.3,$$

significantly exceeding typical Solar System comet values [23]. Elevated CO abundance

$$CO/H_2O = 1.65 \pm 0.09$$

and pronounced red spectral slopes further characterize the object [24].

In standard interpretations, this composition is attributed to galactic cosmic ray (GCR) processing of surface layers. Laboratory studies show that irradiation can convert CO into CO_2 and produce organic-rich crusts. The observed outgassing is therefore thought to sample only a shallow processed layer (~15–20 m), rather than pristine interior material.

This interpretation implies that long-residence interstellar objects primarily expose radiation-processed material rather than original formation signatures.

8.3. Coma Composition and Dust Properties

The coma of **C/2025 N1** (ATLAS) exhibits:

- strong and evolving outgassing (see, e.g. [25]-[28]),
- dominance of relatively large (~100 μm) dust grains [29],
- chemically complex molecular composition.

Detected species include (see, e.g. [30]-[38]):

- **Optical:** CN, Ni
- **Radio:** CH_3OH, HCN
- **Infrared:** H_2O, CO_2, CO, CH_4

Post-perihelion evolution shows:

- increasing CO production,
- emergence of organic emission bands (3.2–3.4 μm),
- asymmetry in H_2O production rates.

A key observational result is the elevated CO_2/H_2O ratio, significantly above typical cometary values.

Key question: What is the origin of the complex chemistry and large dust grains? Within conventional models, these properties are attributed to primordial composition modified by irradiation. Within WUC, they arise from ongoing internal processes associated with the nucleus.

8.4. Sun-Facing Plume and Rotational Modulation

During mid-2025, the coma exhibited a pronounced **sunward-directed plume**, distinct from the classical anti-solar tail [23], [24], [25], [31], [39], [40]. This feature:

- originates from localized activity on the illuminated hemisphere,
- is consistent with anisotropic emission of large dust particles,
- resembles behavior observed in **C/2014 UN271** (Bernardinelli–Bernstein) [41].

Subsequent observations revealed [42], [43]:

- a persistent sunward plume linked to a localized active region,
- a faint high-latitude jet in the inner coma,
- periodic modulation of jet orientation.

The inferred rotation period is:

$$P_{\mathrm{rot}} = 15.48 \pm 0.70 \text{ h},$$

consistent with independent photometric estimates.

This represents one of the clearest detections of rotationally modulated jet activity in a cometary coma.

8.5. WUC Interpretation of Observations

Within the framework of World–Universe Cosmology, the same observational dataset admits a fundamentally different interpretation:

1. Internal Chemical Production

Molecular species are generated by ongoing processes associated with Universe-Created Particles (UCPs), rather than being solely primordial. The observed composition reflects active internal chemistry.

2. Coma as a Self-Annihilating Reactor (SAR) Output

The coma is continuously replenished by internally generated gas and dust:

- no requirement for preserved "pristine" material,
- **sustained activity independent of heliocentric distance**.

3. X-ray Emission Mechanism

X-ray emission may include contributions from:

- gamma radiation produced by UCPs self-annihilation,
- subsequent interaction with coma gases.

4. Isotopic and Chemical Anomalies

Observed compositional anomalies are interpreted as signatures of ongoing particle processes rather than evidence of ancient interstellar origin.

Synthesis

The principal observational features of **C/2025 N1** (ATLAS):

- strong non-gravitational acceleration,
- unusual chemical composition,
- dominance of large dust grains,
- persistent activity at large heliocentric distances,

are commonly interpreted as evidence for an interstellar origin and prolonged cosmic-ray processing.

Within WUC, these same features are instead understood as intrinsic properties of a Solar System Small Body (SB3) characterized by:

- an active UCM nucleus,
- continuous matter and energy production,
- internal conversion of rotational energy into translational motion.

This interpretation provides a unified explanation of both the dynamical and physical properties of the object without invoking an interstellar origin.

9. WUC Explanation of 3I/ATLAS Observations

The full set of observations of **C/2025 N1** (ATLAS) and related small bodies can be interpreted coherently within the framework of World–Universe Cosmology (WUC). In this approach, the dominant factor governing their behavior is not external forcing but **internal physical processes within the nucleus and comae.**

In contrast, explaining the same combination of dynamical and compositional features within standard cosmological and cometary models remains challenging. Within WUC, the observed diversity of chemical compositions, large dust grains, and strongly hyperbolic trajectories emerges naturally from a unified internal mechanism.

9.1. Non-Gravitational Acceleration (NGA)

The non-gravitational acceleration a_{NG} arises from internal energy conversion and is characterized by:

- quasi-constant magnitude,
- weak dependence on heliocentric distance,
- persistence even at large distances where sublimation is negligible.

9.2. Spin Evolution of the Nucleus

The rotational state of the nucleus is expected to evolve through:

- systematic angular momentum loss due to internal processes,
- discrete, step-like changes associated with micro-volcano (MiV) events,
- long-term evolution toward a critical rotation state.

9.3. Coma Composition and Evolution

The coma is internally generated and its composition exhibits:

- non-solar abundance ratios,
- temporal variability not strictly correlated with heliocentric distance,
- emergence of previously undetected molecular species.

9.4. Dust Grain Properties

Dust production is linked to Micro-world processes, leading to:

- characteristic grain sizes about 10^2 μm,
- continuous replenishment independent of solar heating.

9.5. Sun-Facing Plume

The sunward-directed plume is interpreted as a consequence of **ram-pressure-driven activation**. As the small body moves through the interplanetary medium, compression of the upstream gas leads to adiabatic heating. This increases the effective density within the nucleus, enhancing the efficiency of the self-annihilating reactor (SAR). As a result:

- internal energy release intensifies,

- dust production increases preferentially in the sunward direction,
- a persistent sun-facing plume is generated (see Section 6.4.).

9.6. Activity at Large Heliocentric Distances

Sustained activity is expected at all heliocentric distances, including regions where solar-driven sublimation is negligible. Gas and dust production are therefore intrinsic rather than externally driven.

9.7. X-ray and High-Energy Signatures

X-ray emission is interpreted as arising from:

- interaction of internally generated gamma radiation with coma gases,
- rather than solely from solar wind charge exchange.

9.8. Trajectory Evolution

The trajectory is expected to show:

- systematic deviations from purely gravitational plus outgassing models,
- persistent excess velocity not reproducible by standard non-gravitational laws.

9.9. Broader Population Prediction

WUC predicts that a subset of long-period comets will exhibit:

- anomalously high non-gravitational accelerations,
- unusual chemical compositions,
- similar dynamical signatures indicative of internal energy processes.

9.10. Dark Comets and Low-Albedo Asteroids

“Dark comets” and objects such as ‘Oumuamua are interpreted as small bodies that:

- exhibit measurable non-gravitational acceleration,
- lack visible comae or dust tails.

Their dynamics are explained by the same internal mechanism—conversion of rotational energy of the nucleus into translational kinetic energy.

Extremely low albedo values (0.02–0.08) are attributed to:

- low concentrations of ordinary matter in the surrounding coma,
- dominance of non-luminous or weakly interacting material.

Final Statement

Within the framework of World–Universe Cosmology, internal energy mechanisms are fundamental in governing the dynamical behavior of **C/2025 N1** (ATLAS). These processes are not secondary corrections but primary drivers that determine the object’s origin, evolution, and observable properties. More broadly, they offer a new perspective on Small-Body physics and the processes underlying Solar System formation.

Conclusion

World–Universe Cosmology provides a self-consistent framework capable of describing key cosmological parameters and their interrelations while offering quantitative predictions. In several cases, WUC yields values that align closely with observational data, strengthening its internal coherence.

The model does not claim to explain all cosmological phenomena, nor to constitute a complete and final theory. Substantial further development is required. However, in its current form, WUC offers a viable foundation for a new classical cosmological framework, echoing ideas originally proposed by P. Dirac in 1937.

The Solar System has effectively become an experimental laboratory for astrophysics, providing high-quality observational constraints. Recent advances in observational astronomy open the possibility of testing new physical models at unprecedented levels of precision.

We are entering a new era in astronomy, cosmology, and astrophysics. Continued progress will depend on the willingness to explore alternative frameworks and to confront them with observational data.

Acknowledgments

The author expresses deep gratitude to Alexander Prokhorov and Alexander Manenkov for their pivotal influence on his scientific development.

Special acknowledgment is given to Paul Dirac, whose visionary ideas continue to inspire this work, and to Nikola Tesla for his enduring scientific legacy.

The author thanks Christian Corda for publishing related manuscripts, and Robert Kuhn, Nicholas Percival, and Harry Ricker for valuable comments that improved the clarity and scope of this work.

The author also expresses his deepest gratitude to his wife, Anna Netchitailo, for her unwavering support over many years.

References

[1] Netchitailo, V. (2019) High-Energy Atmospheric Physics: Ball Lightning. *Journal of High Energy Physics, Gravitation and Cosmology*, **5**, 360-374. doi: 10.4236/jhepgc.2019.52020..

[2] Netchitailo, V. (2024) Dark Galaxies, Sun-Earth-Moon Interaction, Tunguska Event—Explained by WUM. *Journal of High Energy Physics, Gravitation and Cosmology*, **10**, 836-853. doi: 10.4236/jhepgc.2024.102052.

[3] Micheli, M., et al. (2018) Non-gravitational acceleration in the trajectory of 1I/2017 U1 (‘Oumuamua). Nature, **559**, 223. https://www.nature.com/articles/s41586-018-0254-4.

[4] Eubanks, T. M., *et al*. (2025) Astrometry with Interplanetary Spacecraft: Determination of the Non-gravitational Accelerations of the Interstellar Object 3I/ATLAS. Res. Notes AAS **9** 329. **DOI** 10.3847/2515-5172/ae2915. https://iopscience.iop.org/article/10.3847/2515-5172/ae2915.

[5] Neukart, F. (2025) Non-Gravitational Acceleration in 3I ATLAS: Constraints on Exotic Volatile Outgassing in Interstellar Comets. arXiv:2511.07450.

[6] Scarmato, T. (2025) Interstellar Interloper 3I/ATLAS: Nucleus Size, Photometry in RGB, Af(rho) and Antitail Structure Analysis. arXiv:2512.22365.

[7] Ahuja, G., and Ganesh S. (2026) Effect of different Non-Gravitational accelerations on the trajectory of Interstellar Comet 3I/ATLAS.

[8] Spada, F., Królikowska, M. and Dones, L. (2026) Systematic and Statistical Uncertainties in the Non-Gravitational Acceleration of 3I/ATLAS. arXiv:2603.00782.

[9] 'Oumuamua (A/2017 U1) (2018) Small-Body Database Lookup. Jet Propulsion Laboratory. https://ssd.jpl.nasa.gov/tools/sbdb_lookup.html#/?sstr=1I%2F2017%20U1.

[10] C/2019 Q4 (Borisov) (2024) Small-Body Database Lookup. Jet Propulsion Laboratory. https://ssd.jpl.nasa.gov/tools/sbdb_lookup.html#/?sstr=2I%2FBorisov.

[11] C/2025 N1 (ATLAS) (2026) Small-Body Database Lookup. Jet Propulsion Laboratory. https://ssd.jpl.nasa.gov/tools/sbdb_lookup.html#/?sstr=3I%2FAtlas.

[12] Oreshko, A.G. (2012) Observation of Dark Spherical Area after Passage of Ball Lightning through Thick Absorbers. https://www.researchgate.net/profile/Alexander_Oreshko/publication/312218738_Observation_of_Dark_Spherical_Area_After_Passage_of_Ball_Lightning_Through_Thick_Absorbers/links/5877307808ae329d6226e786/Observation-of-Dark-Spherical-Area-After-Passage-of-Ball-Lightning-Through-Thick-Absorbers.pdf.

[13] Wolfenstein, L. (1994) Superweak interactions. Comments Nucl.Part.Phys. **21**,, 275. https://cds.cern.ch/record/264313/files/P00023830.pdf. https://inspirehep.net/files/d5b8cbf8d3eb311a9ec6bbad370cd5ae.

[14] Netchitailo, V. (2024) Cosmic Bubbles. *Journal of High Energy Physics, Gravitation and Cosmology*, **10**, 438-453. doi: 10.4236/jhepgc.2024.101029.

[15] Ren, X., *et all.* (2026) Interstellar Object 3I/ATLAS Observed from Mars by China's Tianwen-1 Spacecraft. arXiv:2603.10350.

[16] 3I/ATLAS (2026) Wikipedia. https://en.wikipedia.org/wiki/3I/ATLAS.

[17] Belyakov, M., *et al.* (2026) The Volatile Inventory of 3I/ATLAS as seen with JWST/MIRI. arXiv:2601.22034v1.

[18] The European Space Agency (2026) First glimpse of comet 3I/ATLAS from Juice science camera. https://www.esa.int/ESA_Multimedia/Images/2026/02/First_glimpse_of_comet_3I_ATLAS_from_Juice_science_camera

[19] SETI Institute (2026) 3I/ATLAS: Caught in UV What Europa Clipper Saw When No One Else Could. https://www.seti.org/news/3iatlas-caught-in-uv-what-europa-clipper-saw-when-no-one-else-could/#:~:text=Before%20this%20observation%2C%20it%20was,structures%20rather%20than%20transient%20artifacts.

[20] News Staff (2025) Sci. News. XMM-Newton Offers Incredible X-ray View of Interstellar Comet 3I/ATLAS. https://www.sci.news/astronomy/xmm-newton-x-ray-view-interstellar-comet-3i-atlas-14420.html#:~:text=Astronomers%20using%20ESA's%20XMM%2DNewton,team%20said%20in%20a%20statement.

[21] Mathewson, S. (2025) Scientists detect X-ray glow from interstellar comet 3I/ATLAS extending 250,000 miles into space. SPACE. https://www.space.com/astronomy/comets/scientists-detect-x-ray-glow-from-interstellar-comet-3i-atlas-extending-250-000-out-miles-into-space.

[22] Ishi, D., et al. (2025) X-ray observation of the cometary interloper C/2025 N1 (3I/ATLAS) by XRISM/Xtend. The Astronomer's Telegram. https://www.astronomerstelegram.org/?read=17523.

[23] Maggiolo, R., et al. (2025) Interstellar Comet 3I/ATLAS: Evidence for Galactic Cosmic Ray Processing. arXiv:2510.26308.

[24] Harrington-Pinto, O., et al. (2022) A Survey of CO, CO_2, and H_2O in Comets and Centaurs. *Planet. Sci. J.* **3,** 247. **DOI** 10.3847/PSJ/ac960d.

[25] Bolin, B. T., et al. (2025) Interstellar comet 3I/ATLAS: discovery and physical description. arXiv:2507.05252.

[26] Chandler, C. O., et al. (2025) NSF-DOE Vera C. Rubin Observatory Observations of Interstellar Comet 3I/ATLAS (C/2025 N1). arXiv:2507.13409.

[27] Santana-Ros, T., et al. (2025)Temporal Evolution of the Third Interstellar Comet 3I/ATLAS: Spin, Color, Spectra and Dust Activity.

[28] Seligman, D. Z., et al. (2025) Discovery and Preliminary Characterization of a Third Interstellar Object: 3I/ATLAS. arXiv:2507.02757.

[29] Jewitt, J. and Luu, J. (2025) Pre-perihelion Development of Interstellar Comet 3I/ATLAS. arXiv:2510.18769.

[30] Hoogendam, W. B., et al. (2025) Spatial Profiles of 3I/ATLAS CN and Ni Outgassing from Keck/KCWI Integral Field Spectroscopy. arXiv:2510.11779.

[31] Rahatgaonkar, R., et al. (2025) Very Large Telescope Observations of Interstellar Comet 3I/ATLAS. II. From Quiescence to Glow: Dramatic Rise of Ni i Emission and Incipient CN Outgassing at Large Heliocentric Distances*. arXiv:2508.18382.

[32] Manzano, L. E. M., et al. (2025) Onset of CN Emission in 3I/ATLAS: Evidence for Strong Carbon-Chain Depletion. arXiv:2509.01647.

[33] Roth, N. X., et al. (2025) CHOH and HCN in Interstellar Comet 3I/ATLAS Mapped with the ALMA Atacama Compact Array: Distinct Outgassing Behaviors and a Remarkably High CHOH/HCN Production Rate Ratio. arXiv:2511.20845.

[34] Cordiner, M., et al. (2025) Isotopic Evidence for a Cold and Distant Origin of the Interstellar Object 3I/ATLAS.

arXiv:2603.06911.

[35] Lisse, C. M., et al. (2025) SPHEREx Pre-Perihelion Mapping of H2O, CO2, and CO in Interstellar Object 3I/ATLAS. arXiv:2512.07318.

[36] Lisse, C. M., et al. (2026) SPHEREx Re-Observation of Interstellar Object 3I/ATLAS in December 2025: Detection of Increased Post-Perihelion Activity, Refractory Coma Dust, and New Coma Gas Species. arXiv:2601.06759.

[37] Zhang, Q. and Battams, K. (2025) Rapid Brightening of 3I/ATLAS Ahead of Perihelion.

[38] Tan, H., and Li, J.-Y. (2026) Perihelion Asymmetry in the Water Production Rate of the Interstellar Object3I/ATLAS. arXiv:2601.15443.

[39] Jewitt, D., et al. (2025) Hubble Space Telescope Observations of the Interstellar Interloper 3I/ATLAS. arXiv:2508.02934.

[40] Tonry, J. L., et al. (2025) ATLAS Photometry of Interstellar Object 3I/ATLAS. arXiv:2509.05562.

[41] Sekanina, Z. (1974) On the nature of the anti-tail of Comet Kohoutek (1973f) I. A working model. Icarus, **23**, 502. https://www.sciencedirect.com/science/article/abs/pii/001910357490013X?via%3Dihub.

[42] Serra-Ricart, M., Licandro, J. and Alarcon, M. R. (2026) Pre-perihelion detection of a wobbling high-latitude jet in the interstellar comet 3I/ATLAS. A&A, **705**, L3. DOI https://doi.org/10.1051/0004-6361/202558072.
https://www.aanda.org/articles/aa/full_html/2026/01/aa58072-25/aa58072-25.html.

[43] Sekanina, Z. and Miller, F. D. (1976) On the nature of the anti-tail of Comet Kohoutek (1973f). II. Comparison of the working model with ground-based photographic observations. *Icarus*. **27**.135.

https://www.sciencedirect.com/science/article/abs/pii/0019103576901901?via%3Dihub.